S-acylation stabilizes ligand-induced receptor kinase complex formation during plant pattern-triggered immune signalling.

Charlotte H. Hurst[1,2], Dionne Turnbull[1†], Julien Gronnier[3,4†], Sally Myles[1], Robin L. Pflughaupt[5], Michaela Kopischke[6], Paul Davies[5], Susan Jones[7], Silke Robatzek[6,8], Cyril Zipfel[3,6], Piers A. Hemsley[1,2*]

Affiliations:

[1] Division of Plant Sciences, School of Life Sciences, University of Dundee, Dow Street, Dundee, DD1 5EH, Scotland, UK.

[2] Cell and Molecular Sciences, The James Hutton Institute, Invergowrie, Dundee, DD2 5DA, Scotland, UK.

[3] Institute of Plant and Microbial Biology, Zurich-Basel Plant Science Center, University of Zurich, 8008 Zurich, Switzerland.

[4] Present address - ZMBP Universität Tübingen, Auf der Morgenstelle 32, D-72076 Tübingen, Germany

[5] Medical Research Council Protein Phosphorylation and Ubiquitylation Unit, School of Life Sciences, University of Dundee, Dow Street, Dundee, DD1 5EH, Scotland, UK.

[6] The Sainsbury Laboratory, University of East Anglia, Norwich Research Park, NR4 7UH, Norwich, England, UK.

[7] Information and Computational Sciences, The James Hutton Institute, Invergowrie, Dundee, DD2 5DA, Scotland, UK.

[8] LMU Munich Biocenter, Großhadener Strasse 4, 82152 Planegg, DE.

† These authors contributed equally

* Correspondence: p.a.hemsley@dundee.ac.uk

Summary

Plant receptor kinases are key transducers of physical extracellular stimuli, such as the presence of beneficial or pathogenic microbes or secreted signalling molecules. Receptor kinases are regulated by numerous post-translational modifications. Here, using the bacterial flagellin perceiving receptor kinase FLS2, we show that S-acylation at an evolutionarily conserved cysteine is crucial for function. S-acylation involves the addition of long-chain fatty acids to cysteine residues within proteins, altering their biophysical properties and behaviour within the membrane environment. We observe S-acylation of FLS2 at C-terminal kinase domain cysteine residues within minutes of treatment with flg22 ligand, and in a BAK1 co-receptor dependent manner. We demonstrate that S-acylation is essential for FLS2-mediated immune signalling, including anti-bacterial immunity. Similarly, mutating the corresponding conserved cysteine residue in the immune receptor kinase EFR supressed elf18 mediated signalling. Biochemical analysis of unstimulated and activated FLS2 containing complexes using detergents and native membrane DIBMA nanodiscs indicates that S-acylation assists the stabilization of activated receptor kinase complexes withing the membrane environment to increase signalling efficiency.

Key words

S-acylation; palmitoylation; Receptor-kinase; Receptor-like kinase; FLS2; EFR; microdomain; nanodomain; membrane; Arabidopsis

Introduction

The plasma membrane defines the boundary between the cell interior and the external environment. Receptor kinases (RKs) found in the plasma membrane act as the principle means of perception for most of the stimuli that a plant encounters, such as hormones, signalling peptides or microbe associated molecular patterns (MAMPs). RKs comprise the largest single gene family in plants [1, 2] and are central to current efforts to breed or engineer crops able to withstand emerging pathogen threats, interact with beneficial microbes or better tolerate abiotic stress [3-6]. Understanding the mechanisms and principles underlying the formation and activation of RKs complexes is therefore critical to informing these approaches.

The RK FLAGELLIN SENSING 2 (FLS2) is the receptor for bacterial flagellin and the flagellin-derived peptide flg22 [7], and is an archetype for RK research, particularly in the area of host-microbe interactions. flg22 binding to the extracellular FLS2 leucine-rich repeats promotes interaction with the extracellular leucine-rich repeats of the co-receptor BAK1/SERK3, with flg22 acting as molecular glue between FLS2 and BAK1. Subsequent transphosphorylation of FLS2 by BAK1 initiates a cascade of immune signalling to activate anti-bacterial defence responses. As part of this overall process, flg22 binding by FLS2 has been shown to dictate FLS2 phosphorylation, SUMOylation and ubiquitination state, indicating a high degree of post-translational regulation. FLS2 activation also alters overall complex composition [7-17], biophysical properties [18] and behaviour [19, 20] of the complex. However, the underlying mechanisms and functional relevance of these changes remain unknown.

S-acylation is a reversible post-translational modification, whereby long chain fatty acids are added to cysteine residues by protein S-acyl transferases [21] and removed by acyl-protein thioesterases [22]. This modification can lead to changes in protein trafficking, stability, and turnover. S-acylation has been proposed to drive membrane phase partitioning [23, 24] while changes in protein S-acylation state have been hypothesised to modulate protein-protein and protein-membrane interactions, or even alter protein activation states [25]. However, direct experimental evidence to support these ideas is lacking. We recently discovered that FLS2, alongside all other plant RKs tested, is post-translationally modified by S-acylation [26]. Here we demonstrate that S-acylation of FLS2, at a site conserved in all RKs across plants, acts as a positive regulator of signal transduction. Mechanistically, this appears to be driven by S-acylation induced changes to the physical properties of the protein complex, resulting in enhanced stability within its lipid environment and more efficient signal propagation.

Results

FLS2 undergoes ligand responsive S-acylation.

Our previous analysis of FLS2 identified the juxta-transmembrane (TM) domain cysteines (Cys830,831) as being constitutively S-acylated, but this modification was dispensable for FLS2 function [26]. All RK superfamily members subsequently tested, with or without a juxta-TM S-acylation site homologous to FLS2 $C^{830,831}$, also appear to be S-acylated [26]. This indicates that non-juxta-TM S-acylation sites, potentially conserved in all RKs, exist. Other post-translational modifications affecting FLS2, and the broader RK superfamily, including phosphorylation [27], ubiquitination [11] and SUMOylation [17] are all responsive to ligand binding. Given the dynamic nature of S-acylation [22] we were interested to determine whether FLS S-acylation state is also ligand responsive. In Col-0 wild type plants treated with the eliciting peptide flg22, FLS2 S-acylation increased by almost 60% above basal levels following 20-min exposure to flg22. FLS2 S-acylation subsequently returned to basal levels within 1 h (figures 1A and S1A). Consistent with its ligand-dependency, FLS2 S-acylation was contingent upon the FLS2 co-receptor BAK1 (BRI1-ASSOCIATED KINASE) (figure 1B). Additionally, flg22 induced S-acylation of FLS2 was unaffected in *chc2-1* mutants [15] of clathrin heavy chain 2, indicating that S-acylation occurs before endocytosis (figure 1C). Treatment of Arabidopsis Col-0 plants with elf18, a conserved peptide derived from bacterial elongation factor Tu, recognised by the RK EFR (ELONGATION FACTOR-Tu RECEPTOR) that acts similarly to FLS2 [28], failed to elevate FLS2 S-acylation (figure 1D). This demonstrates that the increase in FLS2 S-acylation is specifically linked to activation of FLS2 signalling and not a general phenomenon related to activation of RK-mediated defence responses.

FLS2 flg22 responsive S-acylation sites are conserved in the wider Receptor kinase superfamily.

FLS2 $C^{830,831}S$ mutants [26] showed a similar elevation of S-acylation in response to flg22 (figure S1B). FLS2 therefore contains S-acylation sites in addition to $C^{830,831}$ that are responsive to ligand perception. While FLS2 $C^{830,831}S$ expressed at native levels in unstimulated Arabidopsis is not S-acylated [26], we noted that FLS2 $C^{830,831}S$ is weakly S-acylated in the absence of flg22 when overexpressed in *Nicotiana benthamiana*. Mutation of FLS2 Cys 1132 and 1135 in addition to Cys 830 and 831 (FLS2 $C^{830,831,1132,1135}S$) abolished FLS2 S-acylation compared to FLS2 $C^{830,831}S$ (figure

1E) when expressed in *N. benthamiana*, suggesting that Cys 1132 and 1135 are sites of S-acylation. Accordingly, *fls2c/proFLS2:FLS2 C^{1132,1135}S* Arabidopsis plants (figure S1C) showed no increase in S-acylation following flg22 treatment (figure 1F). Interestingly, 1-2 conserved cysteine residues at the C-terminus of the kinase domain (corresponding to FLS2 Cys 1132 and/or 1135) are conserved across RKs in *Arabidopsis thaliana* (figure S2) and the broader Streptophyte lineage, suggesting a conserved and important role for these cysteines.

Receptor kinase C-terminal S-acylation enhances early immune signalling through FLS2 and EFR

Consistent with the evolutionarily conserved nature of the FLS2 S-acylated cysteines amongst RKs, *fls2c/proFLS2:FLS2 C^{1132,1135}S* plants are impaired in several aspects of early immune signalling, such as reactive oxygen species production, MAP kinase activation and pathogen responsive gene expression (figure 2A, B, C). Both FLS2 and FLS2 C^{1132,1135}S show similar accumulation at the plasma membrane (figure S3A), lateral membrane mobility (figure S3B, C), and association with REM1.3 nanodomains (figure S3D, E, F), indicating that there is no aberrant basal cellular behaviour of the FLS2 C^{1132,1135}S mutant that could be impacting responses to flg22. To determine whether the conserved C-terminal cysteines have a general role in RK function, we mutated the equivalent cysteine in EFR (Cys975, figure S2) to serine and transiently expressed EFR-GFP [29] and EFR C^{975}S-GFP in *N. benthamiana.* Elicitation of EFR action with elf18 demonstrated that MAP kinase activation and immune gene expression was reduced in EFR C^{975}S-GFP expressing plants compared to EFR-GFP (figure 2C, D). This indicates that mutation of the conserved C-terminal cysteine in both FLS2 and EFR has a similar effect on early outputs. Structural homology modelling of FLS2 indicates that the C^{1132,1135}S mutation does not affect FLS2 kinase domain structure (figure S4). Kinase activity is also dispensable for activation of signalling by EFR [30]. The observed effects of the FLS2 C^{1132,1135}S and EFR C^{975}S mutation on early signalling therefore cannot readily be explained by effects on kinase activity or structure.

FLS2 kinase domain S-acylation is required for sustained signalling and bacterial immunity

Early signalling outputs resulting from bacterial perception by FLS2 lead to longer term sustained responses to promote immunity. In line with decreased early immune responses, later flg22-induced gene expression and physiological outputs, such as *PR1* (PATHOGENESIS-RELATED GENE 1) expression and seedling growth inhibition, were affected in *fls2c/proFLS2:FLS2 C^{1132,1135}S* plants (figure 3A, B). As a result of these cumulative signalling defects, FLS2 C^{1132,1135}S failed to complement the hyper-susceptibility of *fls2* mutant plants to the pathogenic bacterium *Pseudomonas syringae* pv. tomato (*Pto*) DC3000 (figure 3C).

S-acylation of FLS2 stabilizes flg22 induced FLS2-BAK1 signalling complexes within the membrane

Differential solubility in cold non-ionic detergents such as IGEPAL CA-630, leading to formation of detergent soluble or resistant membrane fractions (DSM and DRM respectively), has been used to characteries changes to protein biophysical properties, particularly in the context of protein S-acylation [18, 31]. Following flg22 treatment, FLS2 abundance in cold IGEPAL CA-630 derived DRMs showed a slight reduction, while FLS2 C^{1132,1135}S DRM abundance decreased by ~50% (figure

4A, B). Overall, while FLS2 containing complex solubility in cold IGEPAL CA-630 fractionally increases upon activation, suggesting a change in complex protein composition and/or surrounding membrane order, loss of S-acylation has a dramatic effect. These data indicate that FLS2 S-acylation is a major contributor to the overall biophysical properties of the stimulated FLS2 containing protein complex when considered in the context of its membrane environment.

Assessment of flg22-induced FLS2-BAK1 complex formation by co-immunoprecipitation following solubilisation with cold IGEPAL CA-630 [32] indicated that FLS2-BAK1 interaction was reduced or less stable in FLS2 $C^{1132,1135}S$ mutants (figure 4C). Furthermore, flg22-induced BAK1 S^{612} auto-phosphorylation [33], used as a marker of *in vivo* complex formation, was also consistently weaker in FLS2 $C^{1132,1135}S$-expressing plants (figure 4C), supporting these biochemical observations. DRM and co-immunoprecipitation data combined suggests a role for DRM stabilization of observed FLS2-BAK1 complexes during co-immunoprecipitation. This indicates that FLS2 S-acylation alters the biophysical properties of FLS2 that will in turn impact upon the strength or stability of FLS2-BAK1 interactions in the context of cellular membranes.

In contrast to IGEPAL CA-630, diisobutylene/maleic acid (DIBMA) copolymer disrupts cellular membranes in an unbiased manner and does not form DRM-like fractions. DIBMA disrupts all lipid-lipid, but not protein-protein or protein-lipid, interactions to form native membrane nanodiscs containing proteins and their higher order complexes. Loose conformations of protein transmembrane domains within a complex will therefore show reduced co-purification compared to tightly packed transmembrane domains [34]. Comparing the behaviour of proteins and complexes following solubilization with either IGEPAL CA-630 or DIBMA allows for biochemical character and properties to be determined. Using DIBMA to solubilize flg22-induced FLS2-BAK1 complexes prior to co-immunoprecipitation (figure 4D) indicates that FLS2-BAK1 complexes are stabilized by protein-protein and protein-lipid interactions that are reduced or absent from FLS2 $C^{1132,1135}S$-BAK1 complexes. This indicates that S-acylation induced changes to the physical character of FLS2 promote assembly of a DIBMA resistant complex with tightly packed transmembrane domains.

Discussion

FLS2, a prototypical RK, has been shown here to require flg22 ligand-induced S-acylation at Cys1132,1135 for efficient flg22-triggered signalling and resistance to bacterial infection. FLS2 S-acylation occurs within minutes of flg22 perception and requires the co-receptor BAK1, but precedes FLS2 entry into the endocytic pathway (figure 1). Supporting this timescale, preventing FLS2 S-acylation from occurring impairs early signalling outputs, such as the phosphorylation of MAPK and the production of ROS (figure 2). This failure to activate initial signalling also explains the defects in subsequent signalling outputs such as PR1 induction, growth inhibition and, ultimately, resistance to pathogenic bacteria (figure 3). Sequence analysis of RKs from across the Streptophyte lineages indicate that the S-acylation site identified here at the C-terminus of the FLS2 kinase domain is conserved throughout evolutionary history. Mutation of the equivalent cysteine in EFR (Cys975) recapitulates the defects observed in S-acylation defective FLS2,

indicating a conserved function for this site. Recently the P2K1/DORN1/LecRK-I.9 RK was proposed to undergo de-S-acylation followed by re-S-acylation during immune responses [35]. However, the site proposed is unique to the LecRK family, being distinct in function, location, sequence, and structure to the universally conserved cysteine identified here that is also present in P2K1 but was not considered in the previous work. These data demonstrate that, in common with other post-translational modifications, S-acylation may affect multiple sites within an RK with differing effects on RK function. The position and effect of the S-acylation site identified here at the C-terminus of the FLS2 and EFR kinase domains is highly conserved. This opens up the exciting possibility that S-acylation at the conserved C-terminal kinase site may potentially regulate the function of all RKs across plants in a similar manner to FLS2 and EFR.

RK signalling is initiated by binding of a ligand (e.g., flg22) to its receptor (e.g., FLS2), which then facilitates the binding of a co-receptor (e.g., BAK1/SERK3). While this constitutes the minimal ligand recognition complex, substantial evidence supports a far larger number of proteins being intimately associated with both unstimulated and activated receptors and co-receptors. Indeed, existing data indicates that during the process of activation RKs recruit or eject specific proteins from their complexes [10, 16, 36, 37], but precise molecular mechanisms determining these changes are not known. Live cell imaging of unstimulated FLS2 and BAK1 indicates that complex composition, specifically presence or absence of the RK FERONIA (FER), has marked effects on nanoscale organisation and mobility of in the plasma membrane. In addition, activation of the RK FERONIA (FER) by its ligand RALF23 alters BAK1 organisation and mobility [20]. This indicates that both complex composition, and the activation state of individual components, affects behaviour of the whole complex. Changes in direct protein-protein interaction can be explained by allosteric effects. However, it is also possible that alteration of the immediate lipid environment composition, micro-curvature, or structure, brought about by changes in the biophysical properties of the complex, would act to recruit or exclude proteins based on their solubility and packing in the membrane environment surrounding the complex. This is, in essence, one of the biochemical principles proposed to underlie the formation of membrane nanodomains [38]. Activation of FLS2 by flg22 has been reported to decrease overall plasma membrane fluidity and increase plasma membrane order [39], while changing sterol abundance in the plasma membrane affects all stages of FLS2 signalling [40]. This indicates that membrane composition and structure have profound effects on receptor complex function and supports the principle of protein-lipid interactions affecting or effecting RK function. S-acylation, being a fatty acid-based modification of proteins, has been shown to affect protein biophysical character and behaviour in membrane environments [31, 41]. S-acylation also affects membrane micro-curvature [24], a key theoretical determinant of membrane component partitioning required for nanodomain formation [38]. S-acylation therefore represents an ideal mechanism to not only modulate interactions between RK complexes and their proximal membrane components, but also to effect changes in the composition of both.

Altogether our data suggest that flg22-induced, BAK1-dependent S-acylation influences the biophysical properties of FLS2. Our data supports a model where FLS2 S-acylation changes the

transmembrane domain packing or order within the FLS2 complex and alters the FLS2 complex lipid microenvironment. This process stabilises signalling active FLS2 molecular assemblies. These data therefore provide a mechanistic basis for the observed phenomenon of activation state dependent changes in membrane nanodomain content and organisation described for various RKs, including FLS2 [18, 20, 40, 42].

Acknowledgments

We would like to thank Antje Heese and Paul Birch for critical discussions and advice during the preparation of this manuscript. Ari Sadanandom provided *P. syringae* pv. tomato DC3000. This work was supported by BBSRC EASTBIO-DTP studentship (grant number BB/M010996/1) to SM and PH, BBSRC grants BB/M024911/1 and BB/P007902/1 to PH, Royal Society Grant RG140531 to PH, a Heisenberg fellowship from the Deutsche Forschungsgemeinschaft to SR, the Gatsby Charitable Foundation, the University of Zürich, the European Research Council under the Grant Agreement 773153 (grant IMMUNO-PEPTALK) to CZ, and the European Molecular Biology Organization (EMBO Long-Term Fellowship 438-2018) to JG. SJ was supported by the Scottish Government's Rural and Environment Science and Analytical Services division (RESAS).

Author Contributions:

CRediT statement

CHH: Conceptualization, Methodology, Validation, Formal analysis (Equal), Investigation (Lead), Data curation (Equal), Writing - Review & Editing, Visualization. **DT**: Methodology, Validation, Investigation (Equal), Writing - Review & Editing. **JG**: Methodology, Formal analysis (Equal), Investigation (Equal), Data curation (Equal), Writing - Review & Editing, Visualization, Funding acquisition (Equal). **SM**: Validation, Investigation. **MK**: Investigation. **SJ**: Methodology, Software, Investigation. **SR**: Resources, Writing - Review & Editing, Supervision, Funding acquisition (Equal). **CZ**: Resources, Writing - Review & Editing, Supervision, Funding acquisition (Equal). **PAH**: Conceptualization (Lead), Methodology (Lead), Validation, Formal analysis (Lead), Investigation, Data curation (Lead), Resources, Writing - Original Draft (Lead), Writing - Review & Editing (Lead), Visualization (Lead), Supervision (Lead), Project administration (Lead), Funding acquisition (Equal).

Competing Interest Statement: No competing interests declared.

Figure Legends

Figure 1. FLS2 S-acylation increases upon flg22 perception. **A.** Quantification of changes in FLS2 S-acylation following flg22 (n = 5, green solid line) or water only control (n = 2, blue short dashed line) treatment. S-acylation state is shown relative to T0 (black, long dashed line). Error bars show SEM. Significance of difference between flg22 and water treated at 20 minutes is shown as determined by Student's t-test. **B.** S-acylation of FLS2 in response to flg22 requires BAK1. S-acylation state is shown relative to water treated plants of the same genotype (dashed line). Error bars show SEM, Col-0 +flg22 n=5, Col-0 + H2O n = 2, *bak1-4* n = 4, *chc2-1* n = 2, significant difference to flg22 treated Col-0 as determined by Student's t-test are shown. Data shown in

panels A and B are derived from the same biological repeats, Col-0 controls are therefore shared between panels. **C.** FLS2 undergoes S-acylation in response to flg22 treatment but not elf18. S-acylation state is shown relative to untreated plants (black, dashed line). Error bars show SEM, n = 2, significant differences to flg22 treated Col-0 as determined by Student's t-test are shown. **D.** Mutation of FLS2 Cys1132,1135 to serine abolishes residual S-acylation observed in the FLS2 $C^{830,831}S$ background. EX - indicates S-acylation state, LC - loading control, Hyd - indicates presence (+) or absence (-) of hydroxylamine. **E.** FLS2 $C^{1132,1135}S$ mutants are blocked in flg22 mediated increases in S-acylation. S-acylation state is shown relative to water treated plants of the same genotype (black, dashed line). Error bars show SEM, n=3, significant difference to flg22 treated Col-0 as determined by Student's t-test are shown.

Figure 2. Acute responses to flg22 perception are reduced in FLS2 $C^{1132,1135}S$ expressing plants. **A.** ROS production induced by 100 nM flg22 treatment. Data points are the sum of the 3 highest consecutive readings per sample. n = 10 per genotype. Statistical outliers are shown as open circles. Box shows median and IQR, whiskers show +/- 1.5 x IQR. Statistically significant differences at $p < 0.01$ are indicated (a, b) and were calculated using ANOVA and Tukey HSD tests. **B.** MAPK activation in *fls2/FLS2pro:FLS2* $C^{1132,1135}S$ seedlings in response to 100 nM flg22 as determined over time by immunoblot analysis. pMAPK6/pMAPK3 show levels of active form of each MAPK. MAPK6 indicates total levels of MAPK6 as a loading control. Upper shadow band in MAPK6 blot is RUBISCO detected non-specifically by secondary antibody. **C.** Induction of WRKY40 gene expression after 1 hour treatment with 1 mM flg22 in *fls2/FLS2pro:FLS2* $C^{1132,1135}S$ seedlings as determined by qRT-PCR. **D.** Induction of NbACRE31 gene expression after 3-hour treatment with 1 mM elf18 in EFR-GFP and EFR $C^{975}S$-GFP expressing *N. benthamiana* plants as determined by qRT-PCR. Values were calculated using the $\Delta\Delta_{CT}$ method, error bars represent RQMIN and RQMAX and constitute the acceptable error level for a 95% confidence interval according to Student's t-test. **E.** MAPK activation in EFR-GFP and EFR C975S-GFP expressing N. benthamiana plants in response to 15 minutes treatment with 1 mM elf18 as determined by immunoblot analysis. pSIPK/pWIPK show levels of active form of each MAPK. WIPK indicates total levels of WIPK as a loading control. EFR-GFP and EFR $C^{975}S$-GFP levels are shown as a control for dosage effects on MAPK activation.

Figure 3. FLS2 S-acylation is required for long term immune response outputs **A.** Induction of PR1 gene expression after 24 hours treatment with 1 mM flg22 in *fls2/FLS2pro:FLS2* $C^{1132,1135}S$ seedlings as determined by qRT-PCR. Values were calculated using the $\Delta\Delta_{CT}$ method, error bars represent RQMIN and RQMAX and constitute the acceptable error level for a 95% confidence interval according to Student's t-test. Significant differences in transcript mRNA detected in *fls2/FLS2pro:FLS2* $C^{1132,1135}S$ seedlings compared to Col-0 levels in flg22 treated samples are indicated. Similar data were obtained over 3 biological repeats. **B.** Inhibition of growth after 10 days of 1 mM flg22 treatment is reduced in *fls2/FLS2pro:FLS2* $C^{1132,1135}S$ seedlings. Data are averages of 3 biological replicates, error bars are SEM, significant differences at $p < 0.01$ are indicated (a, b, c) and calculated by ANOVA with Tukey HSD test. **C.** Resistance to *P. syringae* DC3000 infection is impaired by loss of FLS2 S-acylation. Box and whisker plots show data from 7

biological repeats (box denotes median and IQR, whiskers show +/- 1.5 x IQR, outliers are shown as open circles), significant differences at $p < 0.05$ are indicated (a, b, c) and calculated by ANOVA with Tukey HSD test.

Figure 4. FLS2 $C^{1132,1135}S$ shows reduced interaction with BAK1 following flg22 stimulation. **A.** Arabidopsis flg22 treated seedlings were lysed in cold IGEPAL CA-630 buffer and separated into detergent soluble (S) and detergent resistant (R) fractions. Relative partitioning of FLS2 into each fraction was determined by western blotting with anti-FLS2 rabbit polyclonal antibody. Loading and purity of fractions is shown by Ponceau S staining of the membrane. **B.** Quantification of data shown in A from 3 biological repeats. Error bars show SEM, significance was calculated using Student's t-test. **C.** FLS2 was immunoprecipitated from IGEPAL CA-630 solubilised flg22 treated Arabidopsis seedling lysates using anti-FLS2 rabbit polyclonal antibody. BAK1 recovery was assessed using rabbit polyclonal anti-BAK1 antibody. flg22 induced BAK1 autophosphorylation at Ser612 was assessed in input samples using rabbit polyclonal anti-BAK1 pS612 antibody. **D.** FLS2 was immunoprecipitated from DIBMA solubilised flg22 treated Arabidopsis seedling lysates using anti-FLS2 rabbit polyclonal antibody. BAK1 recovery was assessed using rabbit polyclonal anti-BAK1 antibody.

Materials and Methods

Cloning and constructs

Fully functional *$FLS2_{pro}$:FLS2* was made using the described FLS2 promoter and open reading frame [43] with stop codon cloned into pENTR D-TOPO [44]. All *FLS2* mutant variants used were based on this construct and were generated using Q5 site directed mutagenesis kit (NEB) according to the manufacturer's guidelines. *$FLS2_{pro}$:FLS2-3xMYC-EGFP* and *$FLS2_{pro}$:FLS2 $C^{1132,1135}$S-3xMYC-EGFP* were made by yeast recombinatorial cloning using a 3xMYC-EGFP PCR fragment amplified from *$FLS2_{pro}$:FLS2-3xMYC-EGFP* [45] recombined with pENTR D-TOPO $FLS2_{pro}$:FLS2 or pENTR D-TOPO $FLS2_{pro}$:FLS2 $C^{1132,1135}$S. Entry clones were recombined into pK7WG,0 [46] using Gateway technology (ThermoFisher) to generate expression constructs. Expression constructs were transformed into *Agrobacterium tumefaciens* strain GV3101 pMP90 [47] for transformation of either Arabidopsis or *Nicotiana benthamiana*.

Plant lines and growth conditions

All Arabidopsis lines were in the Col-0 accession background. The *fls2* [43], *bak1-4* [48] and *chc2-1* [15] mutants have all been described previously. Transgenic *fls2/$FLS2_{pro}$:FLS2* [44] and *fls2/$FLS2_{pro}$:FLS2 $C^{1132,1135}$S* mutant variant lines were generated by Agrobacterium-mediated floral dip transformation [49]. T_3 homozygous plants were used for all experiments. Plant material for experiments was grown on 0.5x MS medium, 0.8% phytagar under 16:8 light:dark cycles at 20 °C in MLR-350 growth chambers (Panasonic). For transient expression *Nicotiana benthamiana* plants were grown in 16:8 light:dark cycles at 24 °C and used at 4-5 weeks old. A. tumefaciens mediated transient expression was performed as described [50] using an OD600 of 0.1 of each expression construct alongside the p19 silencing suppressor at an OD600 of 0.1. Tissue was harvested 48-60 hours post infiltration.

Eliciting peptides

Flg22 peptide (QRLSTGSRINSAKDDAAGLQIA) was synthesised by Dundee Cell Products (Dundee, UK). Elf18 peptide (Ac-SKEKFERTKPHVNVGTIG) was synthesised by Peptide Protein Research Ltd. (Bishops Waltham, UK).

Seedling growth inhibition

For each biological replicate four days post-germination, 10 seedlings of the named genotypes were transferred to 12-well plates (5 seedlings per well), ensuring the cotyledons were not submerged. Wells contained 2 mL of 0.5x MS liquid medium with or without 1 μM flg22. Seedlings were incubated for 10 days and the fresh weight of pooled seedlings in each genotype for each treatment measured and an average taken. Flg22- treated/untreated weights for each genotype were calculated and presented data is an average of these data over three biological repeats. Fully independent biological repeats were performed over a period of 6 months with each genotype only being present once in each repeat.

MAPK activation

Essentially as for [51]; 6 Arabidopsis seedlings of each genotype 10 days post germination were treated with 100 nM flg22 for the indicated times in 2 mL 0.5x MS medium. The 6 seedlings from each genotype at each time point for each treatment were pooled before further analysis. Fully independent biological repeats were performed over a period of 2 years with each genotype only being present once in each repeat. To assess EFR induced MAPK activation in *N. benthamiana* leaves from 5-week-old plants were transiently transformed by agrobacterium infiltration (OD600 0.1 of each construct plus p19 at OD600 0.1). 60 hours after transformation, 1 μM elf18 peptide in water or water only was infiltrated into the leaf and samples harvested after 15 minutes. Samples were subsequently processed as described [51].

Reactive oxygen species production

Protocol based on Mersmann et al. (2010). Essentially, 10 seedlings of each genotype were grown for 14 days in 100 μL of 0.5x MS medium with 0.5% sucrose, in 96-well plates (PerkinElmer). Conditions were maintained at 22 °C with 12:12 light:dark cycles. Growth medium was exchanged for water with 10 nM flg22 for 1 hour, before replacing with water for a further 1 hour. ROS burst was then induced by replacing with a solution containing 100 nM flg22, 400 nM luminol (Fluka), and 20 μg/mL peroxidase (Sigma). Luminescence in each well was measured every 2 minutes in a Varioskan Lux (Thermo Fisher) for 30 cycles (approx. 1 hour total).

Gene expression analysis

Ten seedlings of each genotype 10 days post-germination were treated with 1 μM flg22 or water for the indicated times. The 10 seedlings from each genotype/treatment at each time point for each treatment were pooled before further analysis. RNA was extracted using RNAeasy Plant kit with on column DNAse digestion according to the manufacturer's instructions (Qiagen). Two micrograms RNA was reverse transcribed using a High-Capacity cDNA Reverse Transcription kit

(Applied Biosystems). All transcripts were amplified using validated gene-specific primers [44]. Expression levels were normalized against *PEX4* (At5g25760) [52]. Each sample was analyses in triplicate (technical repeats) for each primer pair within each biological repeat. Relative quantification (RQ) was achieved using the $\Delta\Delta_{CT}$ (comparative cycle threshold) method [53]. Significant differences between samples were determined from a 95% confidence interval calculated using the t-distribution. Fully independent biological repeats were performed over a period of 2 years with each genotype only being present once in each repeat.

Bacterial infection assays

Infection assays of Arabidopsis lines by *Pseudomonas syringae* pv. tomato DC3000 were performed using seedling flood inoculation assays as described [54].

Western blotting

FLS2 was detected using rabbit polyclonal antisera raised against the C-terminus of FLS2 as previously described [9, 55]. Anti-p44/42 MAPK (Erk1/2) (Cell Signalling Technology #9102) was used to detect phosphorylated MAPK3/6 according to manufacturer's recommendations at 1:2000 dilution. Total Arabidopsis MAPK6 or *N. benthamiana* WIPK was detected using anti-Arabidopsis MPK6 (Sigma A7104) at 1:2000. Rabbit polyclonal antibodies against BAK1 were as described [32] or obtained from Agrisera (AS12 1858) and used at 1:5000 dilution. BAK1 phospho-S612 was detected using polyclonal rabbit antisera as described [33]. HRP conjugated secondary antibodies were used to visualise antibody reacting proteins, and Clean-Blot HRP (Thermo Fisher) secondary antibody was used for immunoprecipitation experiments. Western blots were developed using SuperSignal West pico and femto in a 3:1 ratio by volume and signal captured using a Syngene G:box storm imager and quantitative photon count data stored as Syngene SGD files. Signal intensity was quantified from SGD files using Syngene GeneTools software.

S-acylation assays

S-acylation assays using acyl-biotin exchange (ABE) were performed exactly as described [55]. For flg22-dependent changes in FLS2 S-acylation, 7 seedlings 10 days post germination were transferred to each well of 12-well plates. Each well contained 2 mL 0.5 x MS liquid medium. Seedling were incubated for 24 hours on an orbital mixer (Luckham R100/TW Rotatest Shaker, 38 mm orbit at 75 RPM). Thereafter, 100 µL of 0.5 x MS media containing flg22 was added to give a final flg22 concentration of 10 µM. Seedlings were incubated with continued mixing for the indicated times before harvesting.

Co-immunoprecipitation assays using IGEPAL CA-630

Seedlings grown on solid ½ MS for 30-35 days were transferred to wells of a 6-well plates and grown for 7 days in ½ MS 2 mM MES-KOH, pH 5.8. Thereafter, the seedlings were transferred in beakers containing 40 mL of ½ MS 2 mM MES-KOH, pH 5.8 and subsequently treated with sterile mQ water with or without flg22 (final concentration of 100 nM) and incubated for 10 minutes. The seedlings were then frozen in liquid nitrogen and proteins extracted in 50 mM Tris-HCl pH 7.5, 150 mM NaCl, 10% glycerol, 5 mM dithiothreitol, 1% protease inhibitor cocktail (Sigma

Aldrich), 2 mM Na_2MoO_4, 2.5 mM NaF, 1.5 mM activated Na_3VO_4, 1 mM phenylmethanesulfonyl fluoride and 0.5% IGEPAL for 40 minutes at 4 °C. Lysates were clarified at 10,000 g for 20 minutes at 4 °C and the supernatants were filtered through miracloth. For immunoprecipitations, α-rabbit Trueblot agarose beads (eBioscience) coupled with α-FLS2 antibodies [8] were incubated with the crude extract for 3 hours at 4 °C. Subsequently, beads were washed 3 times (50 mM Tris-HCl pH 7.5, 150 mM NaCl, 1 mM phenylmethanesulfonyl fluoride, 0.1% IGEPAL) before adding Laemmli buffer and incubating for 10 minutes at 95 °C. Protein samples were separated in 10% bisacrylamide gels at 150 V for approximately 2 hours and transferred into activated PVDF membranes at 100 V for 90 minutes. Immunoblotting was performed with antibodies diluted in blocking solution (5% fat-free milk in TBS with 0.1% (v/v) Tween-20). Antibodies used in this study: α-BAK1 [32] (1:5000); α-FLS2 [8] (1:1000); α-BAK1 pS612 [33] (1:3000). Blots were developed with Pierce ECL/ ECL Femto Western Blotting Substrate (Thermo Scientific). The following secondary antibodies were used: anti-rabbit IgG-HRP Trueblot (Rockland, 18-8816-31, dilution 1:10000) for detection of FLS2-BAK1 co-immunoprecipitation or anti-rabbit IgG (whole molecule)–HRP (A0545, Sigma, dilution 1:10000) for all other western blots.

Co-immunoprecipitation assays using Diisobutylene-maleic acid (DIBMA)

For each genotype, 2 x 10 seedlings 10 days post-germination were transferred to each well of 12-well plate containing 2 mL 0.5 x MS liquid medium and incubated for 24 hours on an orbital mixer (Luckham R100/TW Rotatest Shaker, 38 mm orbit at 75 RPM). Thereafter, 100 µL of 0.5 x MS media containing flg22 was added to give a final flg22 concentration of 10 µM. The seedlings were further incubated with continued mixing for 20 minutes prior to harvesting and blotting dry. Tissue was lysed in 500 µl of lysis buffer (50 mM Tris-HCl pH 7.2, 10% v/v glycerol, 150 mM NaCl, 1% w/v DIBMA (Anatrace BMA101), with protease inhibitors (1% v/v, Sigma P9599)) and incubated at room temperature for 1 hour with gentle end-over-end mixing. The lysate was centrifuged at 5,000 g for 1 minute and the supernatant filtered through 2 layers of miracloth and combined with an additional 500 µl of filtered lysis buffer (without DIMBA). The clarified lysate was further centrifuged at 16,000 g for 1 minute and the supernatant applied to Amicon 0.5 mL 100 kDa MWCO spin filtration columns and centrifuged at 14,000 g until the retentate was <50 µl. The retentate was diluted to 500 µl with IP buffer (50 mM Tris-HCl pH 7.2, 10% glycerol, 200 mM L-arginine, with protease inhibitor (0.5% v/v, Sigma P9599) and centrifuged at 14,000 g until the retentate was <50 µl. The spin column was inverted and eluted into a 1.5 mL microfuge tube by centrifugation at 100 g for 1 minute The eluate was diluted to 500 µl with IP buffer, of which 20 µl was retained as an input control. Magnetic protein A beads (20 µl per IP reaction) were coated with 5 µg αFLS2 antibody overnight at 4 °C. The resulting beads were washed for 5 minutes with IP buffer containing 0.5 M NaCl followed by 2 washes with IP buffer and resuspended in IP buffer to 100 µl per IP reaction. The resulting FLS2-coated magnetic protein A beads were added to the DIBMA solubilised protein solution and incubated for 3 hours at room temperature with end-over-end mixing. Thereafter, the beads were washed three times with IP buffer, resuspended in 30 µl 2x LDS sample buffer with 2-mercaptoethanol and incubated at 65 °C for 5 minutes with

shaking at 1000 RPM. The samples were separated on a 7.5% SDS-PAGE gel prior to transfer to PVDF and western blotting.

Detergent resistant membrane preparation

To evaluate flg22-dependent changes in FLS2 detergent resistant membrane occupancy, 7 seedlings 10 days post-germination were transferred to each well of a 12-well plate, of which each well contained 2 mL 0.5 x MS liquid medium. Seedlings were incubated for 24 hours on an orbital mixer (Luckham R100/TW Rotatest Shaker, 38 mm orbit at 75 RPM), after which 100 µL of 0.5 x MS media containing flg22 was added to give a final flg22 concentration of 10 µM. The seedlings were further incubated with continuous mixing as before for 20 minutes before harvesting and snap freezing in liquid nitrogen. All subsequent steps were performed at 4 °C or on ice. The seedlings were then lysed in 0.5 mL ice cold 1% (v/v) IGEPAL CA-630 in 25 mM Tris-HCl pH 7.4, 150 mM NaCl, 2 mM EDTA, and 0.1% (v/v) protease inhibitors (Sigma-Aldrich, P9599). Lysates were clarified at 500 g and filtered through 1 layer of miracloth. The filtrate was centrifuged at 16,000 g for 30 minutes and the supernatant retained as a detergent soluble fraction (DSM) and mixed 3:1 with 4x reducing (2-mercaptoethanol) LDS sample buffer. The detergent resistant pellet (DRM) was gently washed with 1 mL lysis buffer, centrifuged at 16,000 g for 5 minutes, and the supernatant discarded. The resulting pellet was resuspended in 27 µL of 3:1 lysis buffer: 4x reducing LDS sample buffer, after which 25 µL of the DRM and DSM were separated by 7.5% SDS-PAGE and probed using anti-FLS2 polyclonal antibody as described [55].

Variable Angle - Total Internal Reflection Fluorescence (VA-TIRF) microscopy

VA-TIRF microscopy was performed using an inverted Leica GSD equipped with a 160x objective (NA = 1.43, oil immersion), and an Andor iXon Ultra 897 EMCCD camera. Images were acquired by illuminating samples with a 488 nm solid state diode laser, a cube filter with an excitation filter 488/10 and an emission filter 535/50 for FLS2-GFP, and a 532 nm solid state diode laser, a cube filter with an excitation filter 532/10 and an emission filter 600/100 for mRFP-REM1.3. Optimum critical angle was determined as giving the best signal-to-noise.

Single particle tracking analysis

Nicotiana benthamiana plants (14-21 days old) were infiltrated with *Agrobacterium tumefaciens* (strain GV3101) solution of OD = 0.15 and imaged 32 to 40 hours post infiltration. For single particle tracking experiments, image time series were recorded at 20 frames per second (50 ms exposure time) by VA-TIRFM. Analyses were carried out as previously described [19], using the plugin TrackMate 2.7.4 in Fiji. Single particles were segmented frame-by-frame by applying a Laplacian of Gaussian filter and estimated particle size of 0.4 µm. Individual single particle were localized with sub-pixel resolution using a built-in quadratic fitting scheme. Single particle trajectories were reconstructed using a simple linear assignment problem [56] with a maximal linking distance of 0.4 µm and without gap-closing. Only tracks with at least ten successive points (tracked for 500 ms) were selected for further analysis. Diffusion coefficients of individual particles were determined using TraJClassifier [57]. For each particle, the slope of the first four time points of their mean square displacement (MSD) plot was used to calculate their diffusion

coefficient according to the following equation: MSD = (x-x0)2+(y-y0)2 and D = MSD/4t, where x0 and y0 are the initial coordinates, x and y are the coordinates at any given time, and t is the time frame.

Co-localization analyses

Nicotiana benthamiana plants (14-21 days old) were infiltrated with *Agrobacterium tumefaciens* (strain GV3101) solution of OD = 0.2 and imaged 48 hours post infiltration. Images were recorded by VA-TIRFM using 250 ms exposure time. As previously reported [42], we emphasised cluster formation in the presented images by using the 'LoG3D' plugin [58]. Quantitative co-localization analyses of the FLS2-GFP and mRFP-REM1.3 were carried out as previously described [42], with minor modification. Using FiJi, images were subjected to a background subtraction using the "Rolling ball" method (radius = 20 pixels) and smoothed. We selected regions of TIRF micrographs with homogeneous illumination for both FLS2-GFP and mRFP-REM1.3. The Pearson co-localization coefficients were assessed using the JACoP plugin of FIJI [59]. For comparison, we determined values of correlation, which could be observed by chance by calculating the Pearson coefficient after flipping one of the two images.

Structural modelling of FLS2 kinase domain

The FLS2 intracellular domain (amino acids 831-1173) was submitted to the phyre2 [60] server (http://www.sbg.bio.ic.ac.uk/phyre2/) in default settings. The solved BIR2 kinase domain structure (PDB 4L68, residues 272-600) [61] was identified as the best match and FLS2 residues 841-1171 were successfully modelled onto the BIR2 structure (confidence 100%, coverage 89%). Cys to Ser mutational effects were modelled using Missense3D [62] in default settings.

Supplemental Figure Legends

Supplemental figure 1. A. Example western blot from Col-0 plants treated with or without flg22 used to generate data shown in Figure 1. FLS2 S-acylation state is shown as a function of recovery on thiopropyl-Sepharose beads in the presence of hydroxylamine (EX+). Samples lacking hydroxylamine (EX-) demonstrate completeness of blocking and lack of background or non-specific binding. LC lanes act as input loading controls for standardisation. **B.** Quantification of changes in FLS2 and FLS2 $C^{830,831}S$ S-acylation following flg22 treatment or water only control (n = 2, blue short dashed line) treatment. flg22 induced changes in S-acylation state are shown relative to water only treatment (black dashed line). Col-0 n = 5, FLS2 $C^{830,831}S$ n = 2, error bars show SEM. Significance of difference in S-acylation state change between FLS2 (Col-0) and FLS2 $C^{830,831}S$ is shown as determined by Student's t-test. **C.** Expression levels of FLS2 $C^{1132,1135}S$ in *fls2/FLS2pro:FLS2 FLS2* $C^{1132,1135}S$ transgenic lines used in this study. 50 mg total protein from 7-day old seedlings was loaded per lane. MYH9.5 is a previously reported cross-reacting protein with the primary anti-FLS2 antibody used.

Supplemental figure 2. Alignment of a representative member from each of the wider Arabidopsis RK superfamilies, centred on the conserved C[X]7RP motif found in the loop between the G- and H-helices of the kinase domain. Putative S-acylation site cysteines are highlighted in teal.

Supplemental figure 3. FLS2-3xMyc-GFP and FLS2 $C^{1132,1135}S$-3xMyc-GFP behave similarly when expressed in N. benthamiana in the absence of flg22. **A.** Fluorecence intensity measurements at the plasma membrane of single cells using TIRF microscopy. Box plot shows median and IQR, whiskers indicate 1.5 x IQR. FLS2-3xMyc-GFP n = 59, FLS2 $C^{1132,1135}S$-3xMyc-GFP n = 42. p value calculated using Student's t-test. Statistical outliers are indicated by open circles. **B.** Single particle tracking of FLS2-3xMyc-GFP and FLS2 $C^{1132,1135}S$-3xMyc-GFP at the plasma membrane using TIRF microscopy. **C.** Quantification of data in B. Box plot shows median and IQR, whiskers indicate 1.5 x IQR. n = 13, p value calculated using Student's t-test. Statistical outliers are indicated by open circles. **D.** FLS2-3xMyc-GFP and FLS2 $C^{1132,1135}S$-3xMyc-GFP form nanodomains in the plasma membrane and show similar co-localisation with mRFP-REM1.3 nanodomains when transiently expressed in N. benthamiana in the absence of flg22. Representative micrographs of FLS2-3xMyc-GFP and FLS2 $C^{1132,1135}S$-3xMyc-GFP (green) co-localisation with mRFP-REM1.3 (magenta) at the plasma membrane of single epidermal cells using TIRF microscopy. **E.** Quantification of FLS2-3xMyc-GFP or FLS2 $C^{1132,1135}S$-3xMyc-GFP co-localisation with mRFP-REM1.3 at the plasma membrane of single epidermal cells. FLS2-3xMyc-GFP n = 14, FLS2 $C^{1132,1135}S$-3xMyc-GFP n = 12. Box plot shows median and IQR, whiskers indicate 1.5 x IQR. p value calculated using Student's t-test. **F.** To determine whether measured co-localisation values shown in B (original) were significant, co-localisation analysis was repeated after rotation of the mRFP-REM1.3 image by 90 degrees (rotated). In all cases, co-localisation was reduced and overall, significantly different, indicating that the co-localisation observed in B is both specific and significant. p values were calculated using Student's t-test.

Supplemental figure 4. Mutation of kinase domain S-acylation site cysteines to serine in FLS2 is not predicted to affect kinase domain structure. **A.** Superimposition of the modelled structures of FLS2 (white) and FLS2 $C^{1132,1135}S$ (blue) kinase domains. B. Zoomed in view of Cys1132,1135 in FLS2 (yellow) and substituted serine (red) residues in FLS2 $C^{1132,1135}S$. Only the proton of Ser1132 is predicted to diverge from the FLS2 structure, being rotated by ~110 degrees compared to the original cysteine. This rotation does not affect the position or packing of any other amino acid.

References

1. Shiu, S.H., and Bleecker, A.B. (2001). Receptor-like kinases from Arabidopsis form a monophyletic gene family related to animal receptor kinases. PNAS *98*, 10763-10768.
2. Shiu, S.H., and Bleecker, A.B. (2003). Expansion of the receptor-like kinase/Pelle gene family and receptor-like proteins in Arabidopsis. Plant Physiol *132*, 530-543.
3. Divi, U.K., and Krishna, P. (2009). Brassinosteroid: a biotechnological target for enhancing crop yield and stress tolerance. N Biotechnol *26*, 131-136.
4. Lacombe, S., Rougon-Cardoso, A., Sherwood, E., Peeters, N., Dahlbeck, D., van Esse, H.P., Smoker, M., Rallapalli, G., Thomma, B.P., Staskawicz, B., et al. (2010). Interfamily transfer of a plant pattern-recognition receptor confers broad-spectrum bacterial resistance. Nature biotechnology *28*, 365-369.
5. Gust, A.A., Brunner, F., and Nurnberger, T. (2010). Biotechnological concepts for improving plant innate immunity. Curr Opin Biotechnol *21*, 204-210.

6. Marshall, A., Aalen, R.B., Audenaert, D., Beeckman, T., Broadley, M.R., Butenko, M.A., Cano-Delgado, A.I., de Vries, S., Dresselhaus, T., Felix, G., et al. (2012). Tackling drought stress: receptor-like kinases present new approaches. Plant Cell *24*, 2262-2278.
7. Gomez-Gomez, L., and Boller, T. (2000). FLS2: an LRR receptor-like kinase involved in the perception of the bacterial elicitor flagellin in Arabidopsis. Mol Cell *5*, 1003-1011.
8. Chinchilla, D., Zipfel, C., Robatzek, S., Kemmerling, B., Nurnberger, T., Jones, J.D., Felix, G., and Boller, T. (2007). A flagellin-induced complex of the receptor FLS2 and BAK1 initiates plant defence. Nature *448*, 497-500.
9. Heese, A., Hann, D.R., Gimenez-Ibanez, S., Jones, A.M., He, K., Li, J., Schroeder, J.I., Peck, S.C., and Rathjen, J.P. (2007). The receptor-like kinase SERK3/BAK1 is a central regulator of innate immunity in plants. PNAS *104*, 12217-12222.
10. Lu, D., Wu, S., Gao, X., Zhang, Y., Shan, L., and He, P. (2010). A receptor-like cytoplasmic kinase, BIK1, associates with a flagellin receptor complex to initiate plant innate immunity. PNAS *107*, 496-501.
11. Lu, D., Lin, W., Gao, X., Wu, S., Cheng, C., Avila, J., Heese, A., Devarenne, T.P., He, P., and Shan, L. (2011). Direct ubiquitination of pattern recognition receptor FLS2 attenuates plant innate immunity. Science *332*, 1439-1442.
12. Spallek, T., Beck, M., Ben Khaled, S., Salomon, S., Bourdais, G., Schellmann, S., and Robatzek, S. (2013). ESCRT-I mediates FLS2 endosomal sorting and plant immunity. PLoS Genet *9*, e1004035.
13. Smith, J.M., Leslie, M.E., Robinson, S.J., Korasick, D.A., Zhang, T., Backues, S.K., Cornish, P.V., Koo, A.J., Bednarek, S.Y., and Heese, A. (2014). Loss of Arabidopsis thaliana Dynamin-Related Protein 2B reveals separation of innate immune signaling pathways. PLoS Pathog *10*, e1004578.
14. Kadota, Y., Sklenar, J., Derbyshire, P., Stransfeld, L., Asai, S., Ntoukakis, V., Jones, J.D., Shirasu, K., Menke, F., Jones, A., et al. (2014). Direct regulation of the NADPH oxidase RBOHD by the PRR-associated kinase BIK1 during plant immunity. Mol Cell *54*, 43-55.
15. Mbengue, M., Bourdais, G., Gervasi, F., Beck, M., Zhou, J., Spallek, T., Bartels, S., Boller, T., Ueda, T., Kuhn, H., et al. (2016). Clathrin-dependent endocytosis is required for immunity mediated by pattern recognition receptor kinases. PNAS *113*, 11034-11039.
16. Stegmann, M., Monaghan, J., Smakowska-Luzan, E., Rovenich, H., Lehner, A., Holton, N., Belkhadir, Y., and Zipfel, C. (2017). The receptor kinase FER is a RALF-regulated scaffold controlling plant immune signaling. Science *355*, 287-289.
17. Orosa, B., Yates, G., Verma, V., Srivastava, A.K., Srivastava, M., Campanaro, A., De Vega, D., Fernandes, A., Zhang, C., Lee, J., et al. (2018). SUMO conjugation to the pattern recognition receptor FLS2 triggers intracellular signalling in plant innate immunity. NatComms *9*, 5185.
18. Keinath, N.F., Kierszniowska, S., Lorek, J., Bourdais, G., Kessler, S.A., Asano, H., Grossniklaus, U., Schulze, W., Robatzek, S., and Panstruga, R. (2010). PAMP-induced changes in plasma membrane compartmentalization reveal novel components of plant immunity. JBC *285*, 39140-39149.
19. Gronnier, J., Franck, C.M., Stegmann, M., DeFalco, T.A., Cifuentes, A.A., Dünser, K., Lin, W., Yang, Z., Kleine-Vehn, J., Ringli, C., et al. (2020). FERONIA regulates FLS2 plasma membrane nanoscale dynamics to modulate plant immune signaling. bioRxiv.
20. Gronnier, J., Franck, C.M., Stegmann, M., DeFalco, T.A., Abarca, A., von Arx, M., Dunser, K., Lin, W., Yang, Z., Kleine-Vehn, J., et al. (2022). Regulation of immune receptor kinase plasma membrane nanoscale organization by a plant peptide hormone and its receptors. Elife *11*.

21. Hemsley, P.A., Kemp, A.C., and Grierson, C.S. (2005). The TIP GROWTH DEFECTIVE1 S-acyl transferase regulates plant cell growth in Arabidopsis. Plant Cell *17*, 2554-2563.
22. Martin, B.R., Wang, C., Adibekian, A., Tully, S.E., and Cravatt, B.F. (2011). Global profiling of dynamic protein palmitoylation. NatMet *9*, 84-89.
23. Hurst, C.H., and Hemsley, P.A. (2015). Current perspective on protein S-acylation in plants: more than just a fatty anchor? Journal of Experimental Botany *66*, 1599-1606.
24. Mesquita, F.S., Abrami, L., Sergeeva, O., Turelli, P., Qing, E., Kunz, B., Raclot, C., Paz Montoya, J., Abriata, L.A., Gallagher, T., et al. (2021). S-acylation controls SARS-CoV-2 membrane lipid organization and enhances infectivity. Dev Cell *56*, 2790-2807 e2798.
25. Turnbull, D., and Hemsley, P.A. (2017). Fats and function: protein lipid modifications in plant cell signalling. Curr Opin Plant Biol *40*, 63-70.
26. Hurst, C.H., Wright, K.M., Turnbull, D., Leslie, K., Jones, S., and Hemsley, P.A. (2019). Juxta-membrane S-acylation of plant receptor-like kinases is likely fortuitous and does not necessarily impact upon function. Sci Rep *9*, 12818.
27. Wang, Y., Li, Z., Liu, D., Xu, J., Wei, X., Yan, L., Yang, C., Lou, Z., and Shui, W. (2014). Assessment of BAK1 activity in different plant receptor-like kinase complexes by quantitative profiling of phosphorylation patterns. J Proteomics *108*, 484-493.
28. Zipfel, C., Kunze, G., Chinchilla, D., Caniard, A., Jones, J.D., Boller, T., and Felix, G. (2006). Perception of the bacterial PAMP EF-Tu by the receptor EFR restricts Agrobacterium-mediated transformation. Cell *125*, 749-760.
29. Holton, N., Nekrasov, V., Ronald, P.C., and Zipfel, C. (2015). The phylogenetically-related pattern recognition receptors EFR and XA21 recruit similar immune signaling components in monocots and dicots. PLoS Pathog *11*, e1004602.
30. Bender, K.W., Couto, D., Kadota, Y., Macho, A.P., Sklenar, J., Bjornson, M., Petriello, A., Farre, M.F., Schwessinger, B., Ntoukakis, V., et al. (2021). ACTIVATION LOOP PHOSPHORYLATION OF A NON-RD RECEPTOR KINASE INITIATES PLANT INNATE IMMUNE SIGNALING. bioRxiv.
31. Abrami, L., Leppla, S.H., and van der Goot, F.G. (2006). Receptor palmitoylation and ubiquitination regulate anthrax toxin endocytosis. J Cell Biol *172*, 309-320.
32. Roux, M., Schwessinger, B., Albrecht, C., Chinchilla, D., Jones, A., Holton, N., Malinovsky, F.G., Tor, M., de Vries, S., and Zipfel, C. (2011). The Arabidopsis leucine-rich repeat receptor-like kinases BAK1/SERK3 and BKK1/SERK4 are required for innate immunity to hemibiotrophic and biotrophic pathogens. Plant Cell *23*, 2440-2455.
33. Perraki, A., DeFalco, T.A., Derbyshire, P., Avila, J., Sere, D., Sklenar, J., Qi, X., Stransfeld, L., Schwessinger, B., Kadota, Y., et al. (2018). Phosphocode-dependent functional dichotomy of a common co-receptor in plant signalling. Nature *561*, 248-252.
34. Oluwole, A.O., Danielczak, B., Meister, A., Babalola, J.O., Vargas, C., and Keller, S. (2017). Solubilization of Membrane Proteins into Functional Lipid-Bilayer Nanodiscs Using a Diisobutylene/Maleic Acid Copolymer. Angew Chem Int Ed Engl *56*, 1919-1924.
35. Chen, D., Hao, F., Mu, H., Ahsan, N., Thelen, J.J., and Stacey, G. (2021). S-acylation of P2K1 mediates extracellular ATP-induced immune signaling in Arabidopsis. NatComms *12*, 2750.
36. Yeh, Y.H., Panzeri, D., Kadota, Y., Huang, Y.C., Huang, P.Y., Tao, C.N., Roux, M., Chien, H.C., Chin, T.C., Chu, P.W., et al. (2016). The Arabidopsis Malectin-Like/LRR-RLK IOS1 is Critical for BAK1-Dependent and BAK1-Independent Pattern-Triggered Immunity. Plant Cell *28*, 1701-1721.
37. Imkampe, J., Halter, T., Huang, S., Schulze, S., Mazzotta, S., Schmidt, N., Manstretta, R., Postel, S., Wierzba, M., Yang, Y., et al. (2017). The Arabidopsis Leucine-Rich Repeat

Receptor Kinase BIR3 Negatively Regulates BAK1 Receptor Complex Formation and Stabilizes BAK1. Plant Cell *29*, 2285-2303.

38. Allender, D.W., Giang, H., and Schick, M. (2020). Model Plasma Membrane Exhibits a Microemulsion in Both Leaves Providing a Foundation for "Rafts". Biophys J *118*, 1019-1031.

39. Sandor, R., Der, C., Grosjean, K., Anca, I., Noirot, E., Leborgne-Castel, N., Lochman, J., Simon-Plas, F., and Gerbeau-Pissot, P. (2016). Plasma membrane order and fluidity are diversely triggered by elicitors of plant defence. JExBot *67*, 5173-5185.

40. Cui, Y., Li, X., Yu, M., Li, R., Fan, L., Zhu, Y., and Lin, J. (2018). Sterols regulate endocytic pathways during flg22-induced defense responses in Arabidopsis. Development *145*.

41. Blaskovic, S., Blanc, M., and van der Goot, F.G. (2013). What does S-palmitoylation do to membrane proteins? FEBS J *280*, 2766-2774.

42. Bucherl, C.A., Jarsch, I.K., Schudoma, C., Segonzac, C., Mbengue, M., Robatzek, S., MacLean, D., Ott, T., and Zipfel, C. (2017). Plant immune and growth receptors share common signalling components but localise to distinct plasma membrane nanodomains. Elife *6*, e25114.

43. Zipfel, C., Robatzek, S., Navarro, L., Oakeley, E.J., Jones, J.D., Felix, G., and Boller, T. (2004). Bacterial disease resistance in Arabidopsis through flagellin perception. Nature *428*, 764-767.

44. Hurst, C.H., Turnbull, D., Myles, S.M., Leslie, K., Keinath, N.F., and Hemsley, P.A. (2018). Variable Effects of C-Terminal Fusions on FLS2 Function: Not All Epitope Tags Are Created Equal. Plant Physiol *177*, 522-531.

45. Robatzek, S., Chinchilla, D., and Boller, T. (2006). Ligand-induced endocytosis of the pattern recognition receptor FLS2 in Arabidopsis. Genes Dev *20*, 537-542.

46. Karimi, M., Inze, D., and Depicker, A. (2002). GATEWAY vectors for Agrobacterium-mediated plant transformation. Trends Plant Sci *7*, 193-195.

47. Koncz, C., and Schell, J. (1986). The promoter of TL-DNA gene 5 controls the tissue-specific expression of chimaeric genes carried by a novel type of Agrobacterium binary vector. Mol. Gen. Genet. *204*.

48. Kemmerling, B., Schwedt, A., Rodriguez, P., Mazzotta, S., Frank, M., Qamar, S.A., Mengiste, T., Betsuyaku, S., Parker, J.E., Mussig, C., et al. (2007). The BRI1-associated kinase 1, BAK1, has a brassinolide-independent role in plant cell-death control. Curr Biol *17*, 1116-1122.

49. Clough, S.J., and Bent, A.F. (1998). Floral dip: a simplified method for Agrobacterium-mediated transformation of Arabidopsis thaliana. PlantJ *16*, 735-743.

50. Turnbull, D., Yang, L., Naqvi, S., Breen, S., Welsh, L., Stephens, J., Morris, J., Boevink, P.C., Hedley, P.E., Zhan, J., et al. (2017). RXLR Effector AVR2 Up-Regulates a Brassinosteroid-Responsive bHLH Transcription Factor to Suppress Immunity. Plant Physiol *174*, 356-369.

51. Schwessinger, B., Roux, M., Kadota, Y., Ntoukakis, V., Sklenar, J., Jones, A., and Zipfel, C. (2011). Phosphorylation-dependent differential regulation of plant growth, cell death, and innate immunity by the regulatory receptor-like kinase BAK1. PLoS Genet *7*, e1002046.

52. Wathugala, D.L., Hemsley, P.A., Moffat, C.S., Cremelie, P., Knight, M.R., and Knight, H. (2012). The Mediator subunit SFR6/MED16 controls defence gene expression mediated by salicylic acid and jasmonate responsive pathways. New Phytologist *195*, 217-230.

53. Schmittgen, T.D., and Livak, K.J. (2008). Analyzing real-time PCR data by the comparative C(T) method. Nat Protoc *3*, 1101-1108.

54. Ishiga, Y., Ishiga, T., Uppalapati, S.R., and Mysore, K.S. (2011). Arabidopsis seedling flood-inoculation technique: a rapid and reliable assay for studying plant-bacterial interactions. Plant Methods *7*, 32.
55. Hurst, C.H., Turnbull, D., Plain, F., Fuller, W., and Hemsley, P.A. (2017). Maleimide scavenging enhances determination of protein S-palmitoylation state in acyl-exchange methods. Biotechniques *62*, 69-75.
56. Jaqaman, K., Loerke, D., Mettlen, M., Kuwata, H., Grinstein, S., Schmid, S.L., and Danuser, G. (2008). Robust single-particle tracking in live-cell time-lapse sequences. NatMet *5*, 695-702.
57. Wagner, T., Kroll, A., Haramagatti, C.R., Lipinski, H.G., and Wiemann, M. (2017). Classification and Segmentation of Nanoparticle Diffusion Trajectories in Cellular Micro Environments. PLoS One *12*, e0170165.
58. Sage, D., Neumann, F.R., Hediger, F., Gasser, S.M., and Unser, M. (2005). Automatic tracking of individual fluorescence particles: application to the study of chromosome dynamics. IEEE Transactions on Image Processing *14*, 1372-1383.
59. Bolte, S., and Cordelieres, F.P. (2006). A guided tour into subcellular colocalization analysis in light microscopy. J Microsc *224*, 213-232.
60. Kelley, L.A., Mezulis, S., Yates, C.M., Wass, M.N., and Sternberg, M.J. (2015). The Phyre2 web portal for protein modeling, prediction and analysis. Nat Protoc *10*, 845-858.
61. Blaum, B.S., Mazzotta, S., Noldeke, E.R., Halter, T., Madlung, J., Kemmerling, B., and Stehle, T. (2014). Structure of the pseudokinase domain of BIR2, a regulator of BAK1-mediated immune signaling in Arabidopsis. J Struct Biol *186*, 112-121.
62. Ittisoponpisan, S., Islam, S.A., Khanna, T., Alhuzimi, E., David, A., and Sternberg, M.J.E. (2019). Can Predicted Protein 3D Structures Provide Reliable Insights into whether Missense Variants Are Disease Associated? J Mol Biol *431*, 2197-2212.

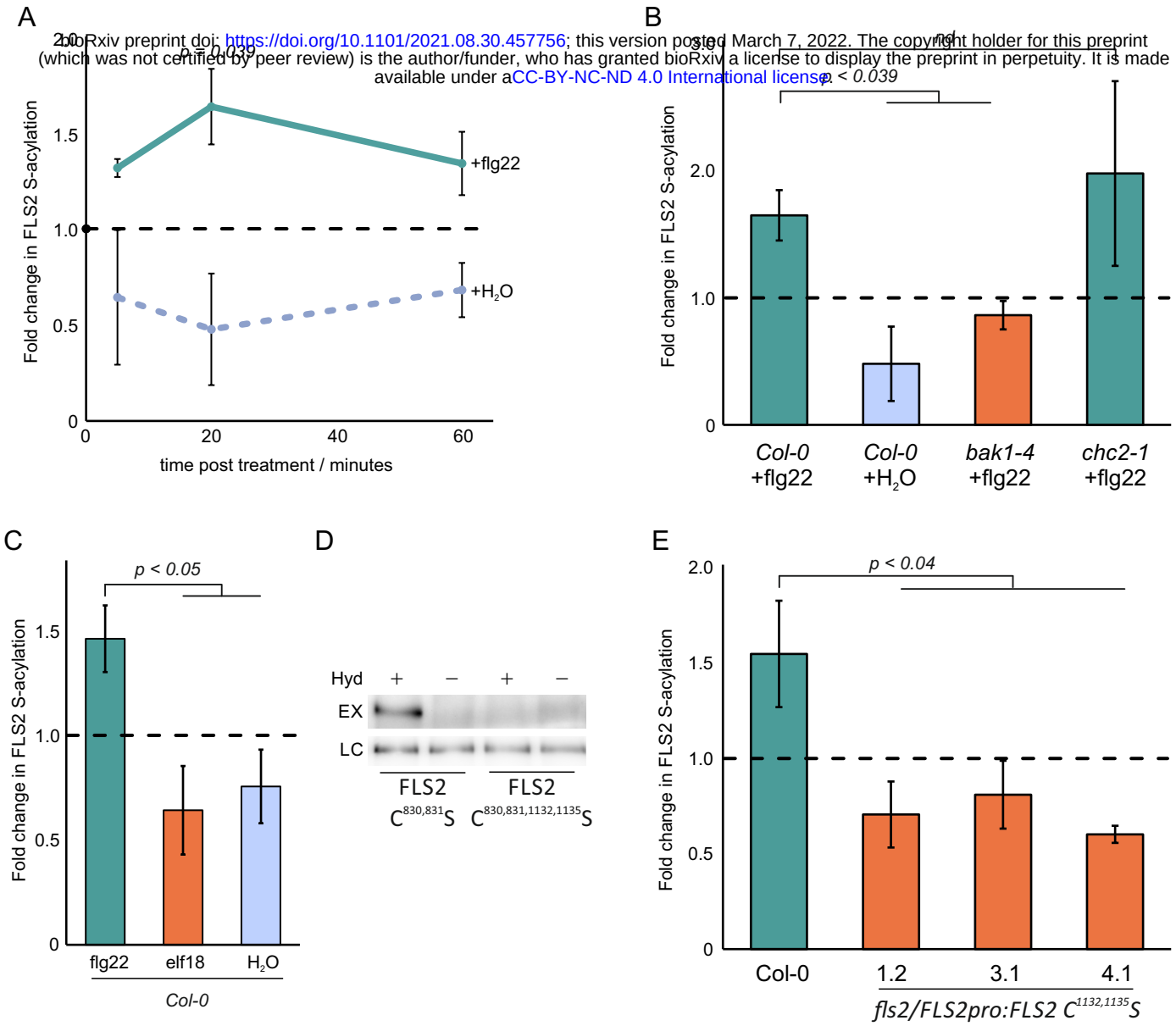

Figure 1. FLS2 S-acylation increases upon flg22 perception. A. Quantification of changes in FLS2 S-acylation following flg22 (n = 5, green solid line) or water only control (n = 2, blue short dashed line) treatment. S-acylation state is shown relative to T_0 (black, long dashed line). Error bars show SEM. Significance of difference between flg22 and water treated at 20 minutes is shown as determined by Student's t-test. **B.** S-acylation of FLS2 in response to flg22 requires BAK1. S-acylation state is shown relative to water treated plants of the same genotype (dashed line). Error bars show SEM, *Col-0* +flg22 n=5, *Col-0* + H2O n = 2, *bak1-4* n = 4, *chc2-1* n = 2, significant difference to flg22 treated *Col-0* as determined by Student's t-test are shown. Data shown in panels A and B are derived from the same biological repeats, *Col-0* controls are therefore shared between panels. **C.** FLS2 undergoes S-acylation in response to flg22 treatment but not elf18. S-acylation state is shown relative to untreated plants (black, dashed line). Error bars show SEM, n = 2, significant differences to flg22 treated *Col-0* as determined by Student's t-test are shown**. D.** Mutation of FLS2 Cys1132,1135 to serine abolishes residual S-acylation observed in the FLS2 $C^{830,831}S$ background. EX - indicates S-acylation state, LC - loading control, Hyd - indicates presence (+) or absence (-) of hydroxylamine. **E.** FLS2 $C^{1132,1135}S$ mutants are blocked in flg22 mediated increases in S-acylation. S-acylation state is shown relative to water treated plants of the same genotype (black, dashed line). Error bars show SEM, n=3, significant difference to flg22 treated *Col-0* as determined by Student's t-test are shown.

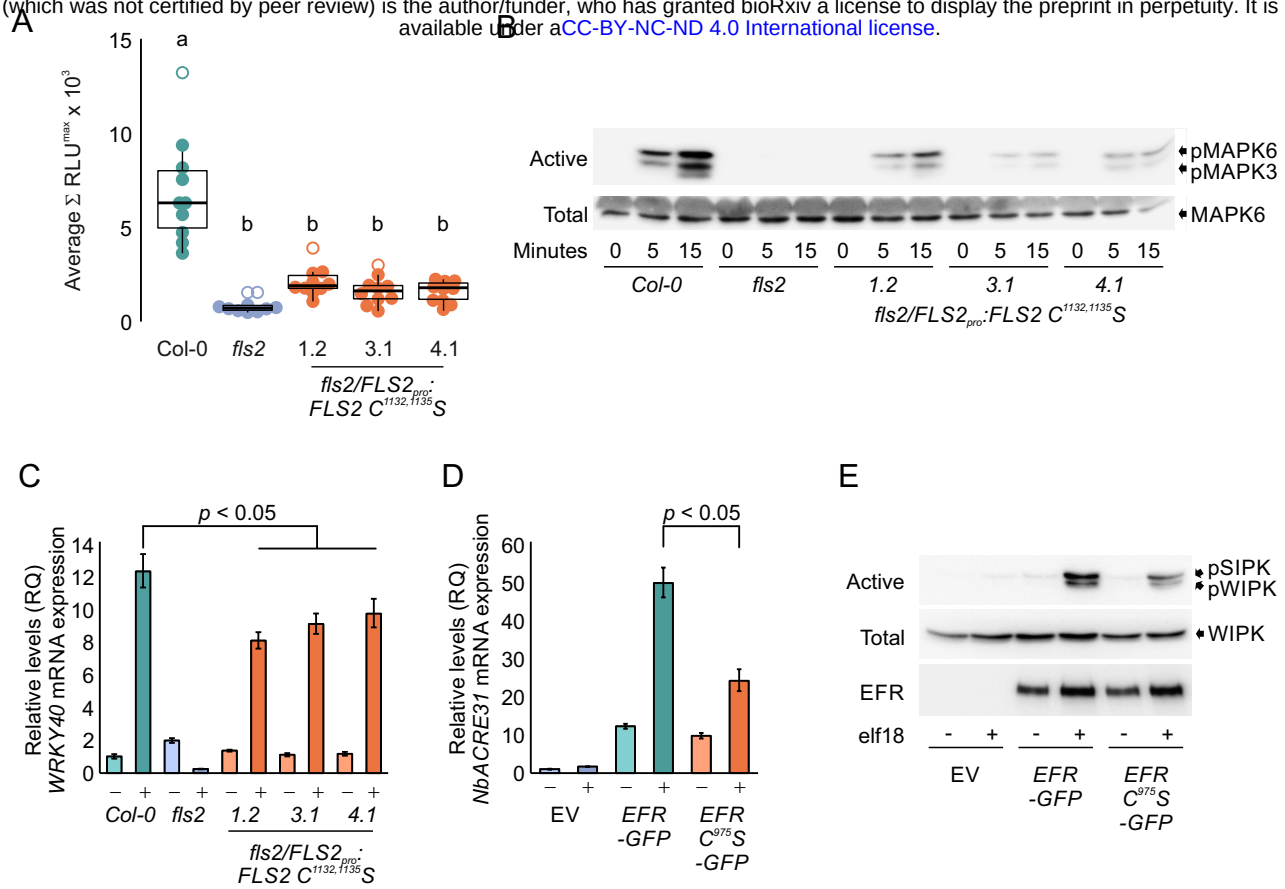

Figure 2. Acute responses to flg22 perception are reduced in FLS2 C^{1132,1135}S expressing plants. A. ROS production induced by 100 nM flg22 treatment. Data points are the sum of the 3 highest consecutive readings per sample. n = 10 per genotype. Statistical outliers are shown as open circles. Box shows median and IQR, whiskers show +/- 1.5 x IQR. Statistically significant differences at p < 0.01 are indicated (a, b) and were calculated using ANOVA and Tukey HSD tests. **B**. MAPK activation in *fls2/FLS2pro:FLS2 C^{1132,1135}S* seedlings in response to 100 nM flg22 as determined over time by immunoblot analysis. pMAPK6/pMAPK3 show levels of active form of each MAPK. MAPK6 indicates total levels of MAPK6 as a loading control. Upper shadow band in MAPK6 blot is RUBISCO detected non-specifically by secondary antibody. **C.** Induction of *WRKY40* gene expression after 1 hour treatment with 1 μM flg22 in *fls2/FLS2pro:FLS2 C^{1132,1135}S* seedlings as determined by qRT-PCR. **D.** Induction of *NbACRE31* gene expression after 3 hour treatment with 1 μM elf18 in *EFR-GFP* and *EFR C^{975}S-GFP* expressing *N. benthamiana* plants as determined by qRT-PCR. Values were calculated using the $\Delta\Delta C_T$ method, error bars represent RQ_{MIN} and RQ_{MAX} and constitute the acceptable error level for a 95% confidence interval according to Student's t-test. **E.** MAPK activation in *EFR-GFP and EFR C^{975}S*-GFP expressing *N. benthamiana* plants in response to 15 minutes treatment with 1 μM elf18 as determined by immunoblot analysis. pSIPK/pWIPK show levels of active form of each MAPK. WIPK indicates total levels of WIPK as a loading control. EFR-GFP and EFR C^{975}S-GFP levels are shown as a control for dosage effects on MAPK activation.

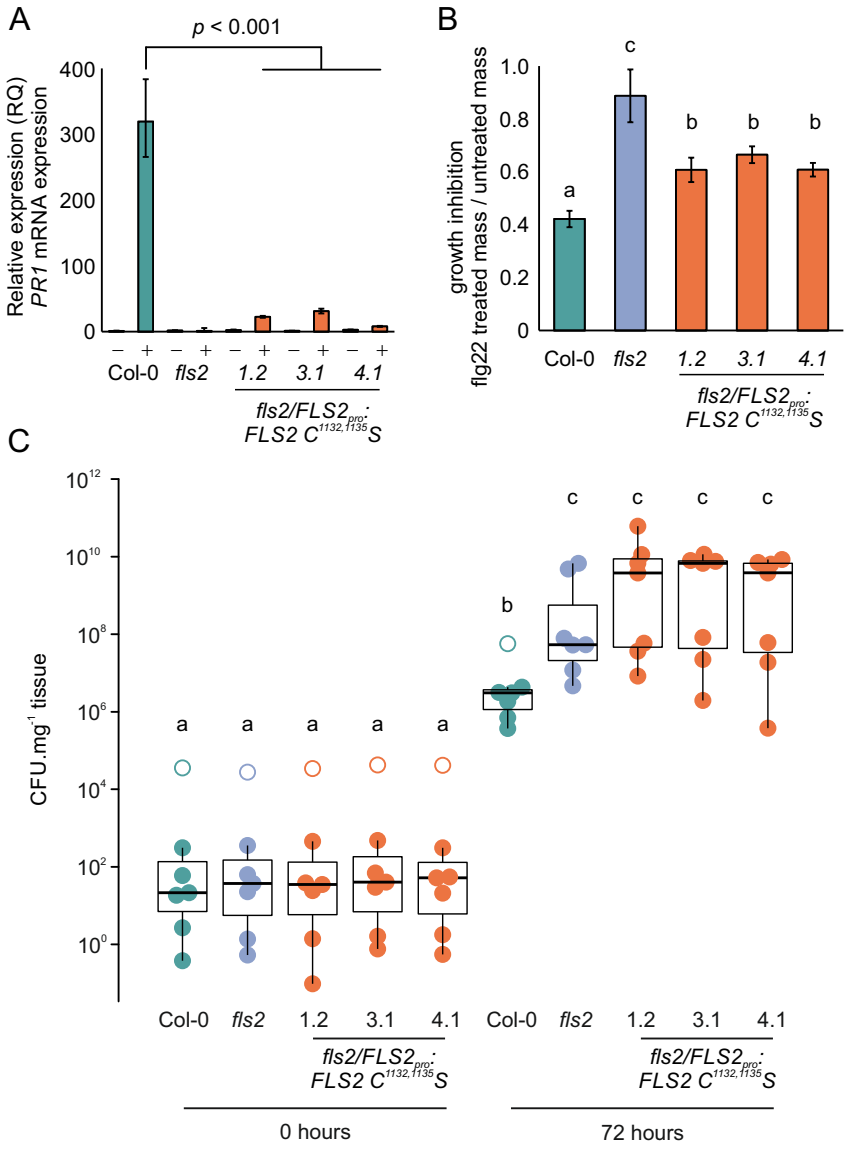

Figure 3. FLS2 S-acylation is required for long term immune response outputs (A). Induction of *PR1* gene expression after 24 hours treatment with 1 μM flg22 in *fls2/FLS2pro:FLS2* $C^{1132,1135}S$ seedlings as determined by qRT-PCR. Values were calculated using the $\Delta\Delta C_T$ method, error bars represent RQMIN and RQMAX and constitute the acceptable error level for a 95% confidence interval according to Student's t-test. Significant differences in transcript mRNA detected in *fls2/FLS2pro:FLS2* $C^{1132,1135}S$ seedlings compared to Col-0 levels in flg22 treated samples are indicated. Similar data were obtained over 3 biological repeats. **(B).** Inhibition of growth after 10 days of 1 μM flg22 treatment is reduced in *fls2/FLS2pro:FLS2* $C^{1132,1135}S$ seedlings. Data are averages of 3 biological replicates, error bars are SEM, significant differences at $p < 0.01$ are indicated (a, b, c) and calculated by ANOVA with Tukey HSD test. **(C).** Resistance to *P. syringae* DC3000 infection is impaired by loss of FLS2 S-acylation. Box and whisker plots show data from 7 biological repeats (box denotes median and IQR, whiskers show +/- 1.5 x IQR, outliers are shown as open circles), significant differences at $p < 0.05$ are indicated (a, b, c) and calculated by ANOVA with Tukey HSD test.

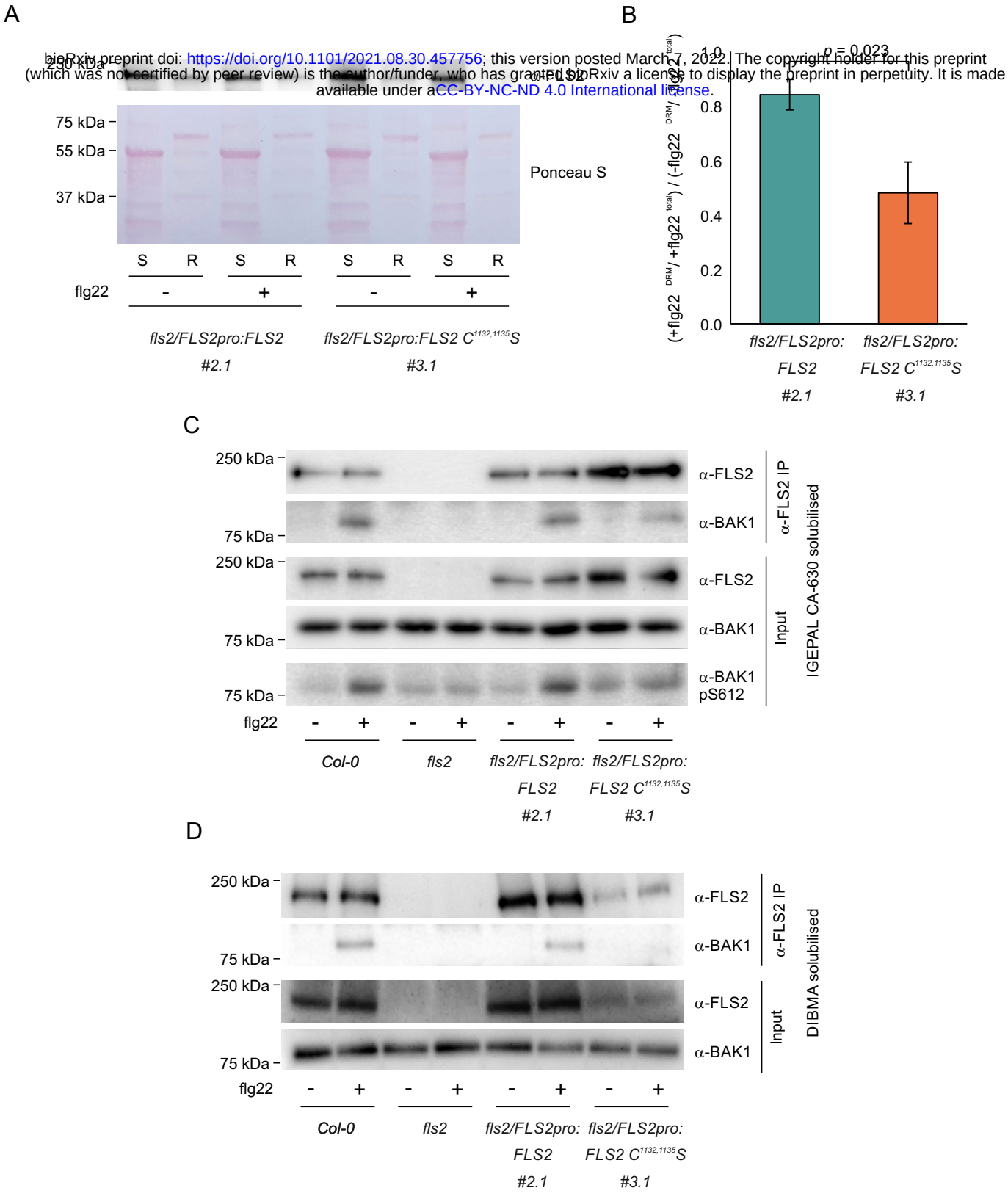

Figure 4. FLS2 $C^{1132,1135}S$ shows reduced interaction with BAK1 following flg22 stimulation. **A.** Arabidopsis flg22 treated seedlings were lysed in cold IGEPAL CA-630 buffer and separated into detergent soluble (S) and detergent resistant (R) fractions. Relative partitioning of FLS2 into each fraction was determined by western blotting with anti-FLS2 rabbit polyclonal antibody. Loading and purity of fractions is shown by Ponceau S staining of the membrane. **B.** Quantification of data shown in A from 3 biological repeats. Error bars show SEM, significance was calculated using Student's t-test. **C.** FLS2 was immunoprecipitated from IGEPAL CA-630 solubilised flg22 treated Arabidopsis seedling lysates using anti-FLS2 rabbit polyclonal antibody. BAK1 recovery was assessed using rabbit polyclonal anti-BAK1 antibody. flg22 induced BAK1 autophosphorylation at Ser612 was assessed in input samples using rabbit polyclonal anti-BAK1 pS612 antibody. **D.** FLS2 was immunoprecipitated from DIBMA solubilised flg22 treated Arabidopsis seedling lysates using anti-FLS2 rabbit polyclonal antibody. BAK1 recovery was assessed using rabbit polyclonal anti-BAK1 antibody.

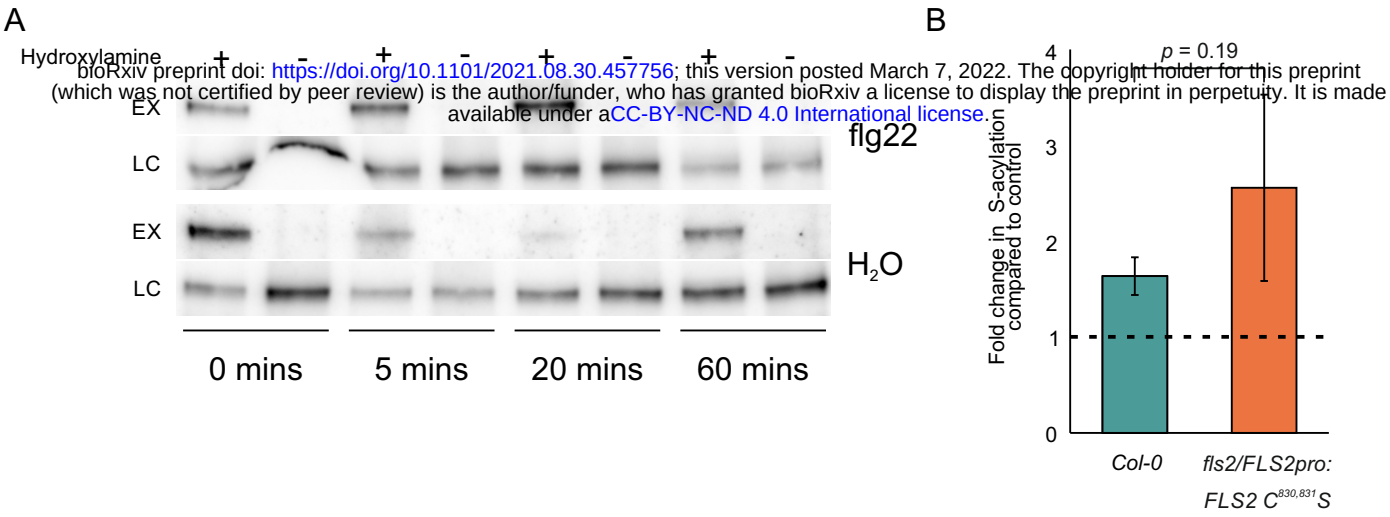

Supplemental figure 1. A. Example western blot from *Col-0* plants treated with or without flg22 used to generate data shown in Figure 1. FLS2 S-acylation state is shown as a function of recovery on thiopropyl-Sepharose beads in the presence of hydroxylamine (EX+). Samples lacking hydroxylamine (EX-) demonstrate completeness of blocking and lack of background or non-specific binding. LC lanes act as input loading controls for standardisation. **B.** Quantification of changes in FLS2 and FLS2 $C^{830,831}S$ S-acylation following flg22 treatment or water only control (n = 2, blue short dashed line) treatment. flg22 induced changes in S-acylation state are shown relative to water only treatment (black dashed line). *Col-0* n = 5, FLS2 $C^{830,831}S$ n = 2, error bars show SEM. Significance of difference in S-acylation state change between FLS2 (*Col-0*) and FLS2 $C^{830,831}S$ is shown as determined by Student's t-test.

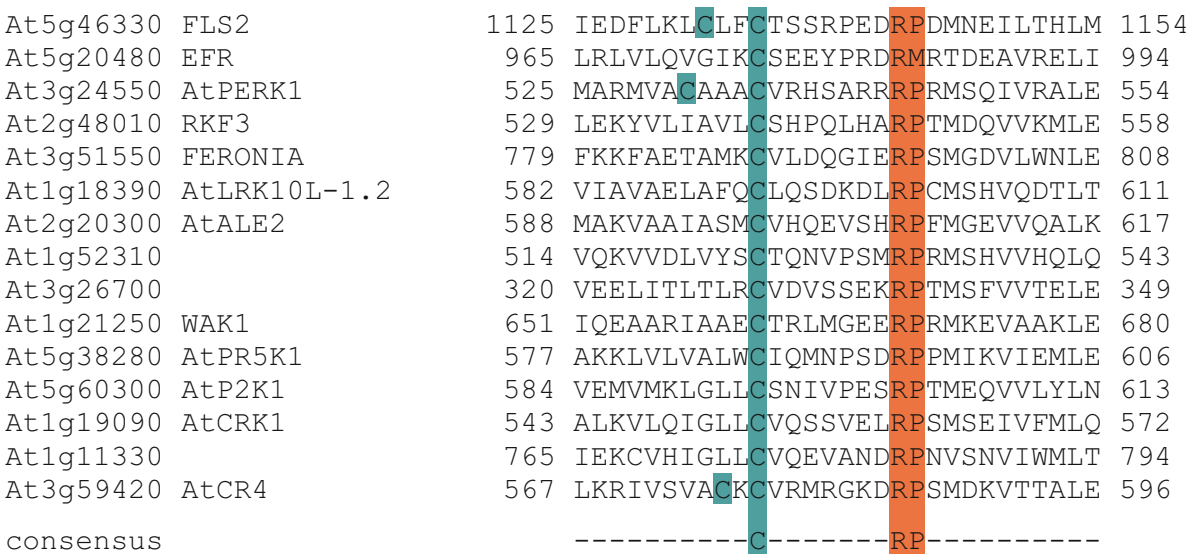

Supplemental figure 2. Alignment of a representative member from each of the wider Arabidopsis RK superfamilies, centred on the conserved C[X]$_7$RP motif found in the loop between the G- and H-helices of the kinase domain. Putative S-acylation site cysteines are highlighted in teal.

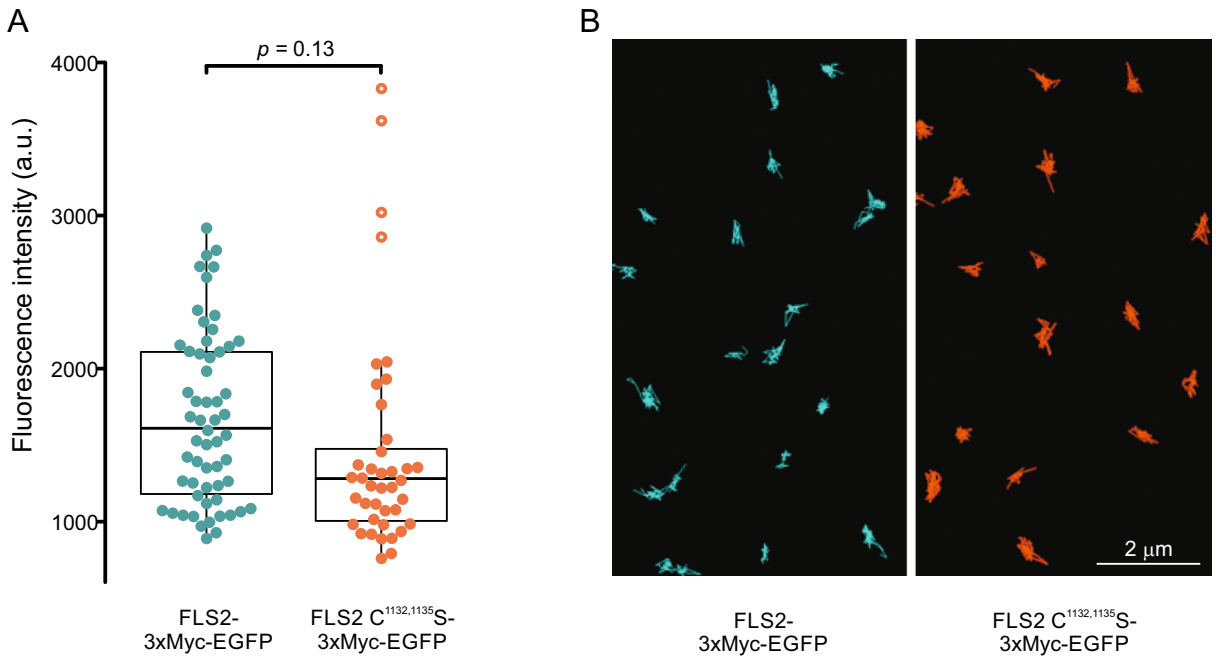

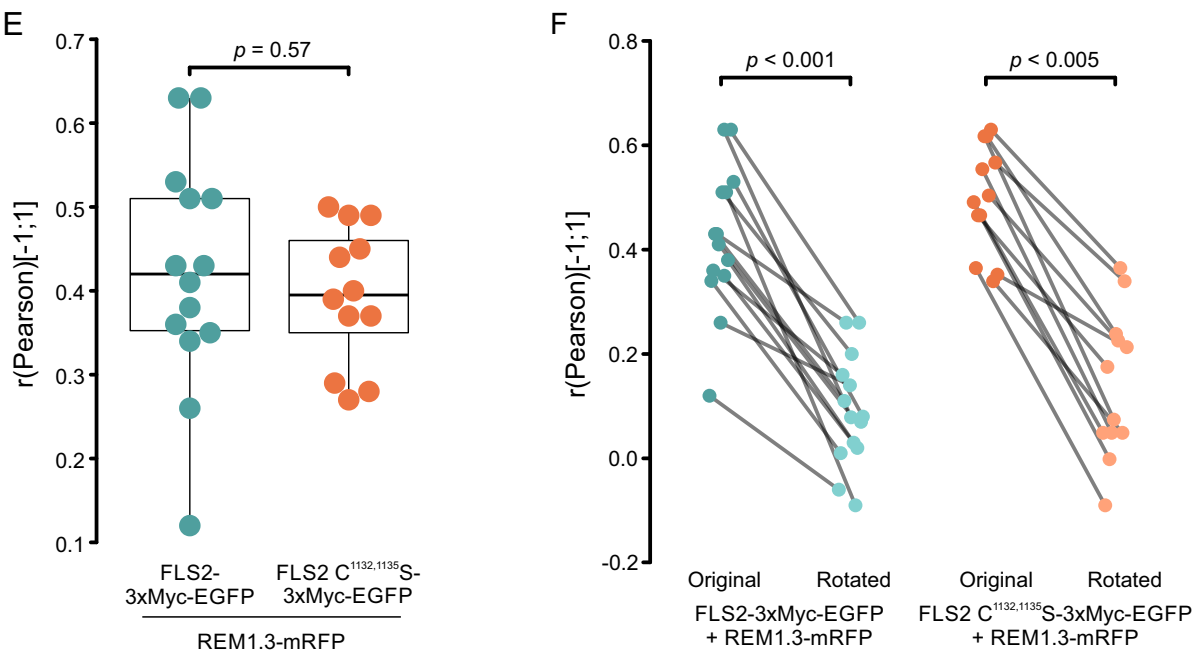

Supplemental figure 3. FLS2-3xMyc-GFP and FLS2 C^{1132,1135}S-3xMyc-GFP behave similarly when expressed in *N. benthamiana* in the absence of flg22. **A.** Fluorecence intensity measurements at the plasma membrane of single cells using TIRF microscopy. Box plot shows median and IQR, whiskers indicate 1.5 x IQR. FLS2-3xMyc-GFP n = 59, FLS2 C^{1132,1135}S-3xMyc-GFP n = 42. *p* value calculated using Student's t-test. Statistical outliers are indicated by open circles. **B.** Single particle tracking of FLS2-3xMyc-GFP and FLS2 C^{1132,1135}S-3xMyc-GFP at the plasma membrane using TIRF microscopy. **C.** Quantification of data in B. Box plot shows median and IQR, whiskers indicate 1.5 x IQR. n = 13, *p* value calculated using Student's t-test. Statistical outliers are indicated by open circles. **D.** FLS2-3xMyc-GFP and FLS2 C^{1132,1135}S-3xMyc-GFP form nanodomains in the plasma membrane and show similar co-localisation with mRFP-REM1.3 nanodomains when transiently expressed in *N. benthamiana* in the absence of flg22. Representative micrographs of FLS2-3xMyc-GFP and FLS2 C^{1132,1135}S-3xMyc-GFP (green) co-localisation with mRFP-REM1.3 (magenta) at the plasma membrane of single epidermal cells using TIRF microscopy. **E.** Quantification of FLS2-3xMyc-GFP or FLS2 C1132,1135S-3xMyc-GFP co-localisation with mRFP-REM1.3 at the plasma membrane of single epidermal cells. FLS2-3xMyc-GFP n = 14, FLS2 C^{1132,1135}S-3xMyc-GFP n = 12**.** Box plot shows median and IQR, whiskers indicate 1.5 x IQR. *p* value calculated using Student's t-test. **F.** To determine whether measured co-localisation values shown in B (original) were significant, co-localisation analysis was repeated after rotation of the mRFP-REM1.3 image by 90 degrees (rotated). In all cases, co-localisation was reduced and overall significantly different, indicating that the co-localisation observed in B is both specific and significant. *p* values were calculated using Student's t-test.

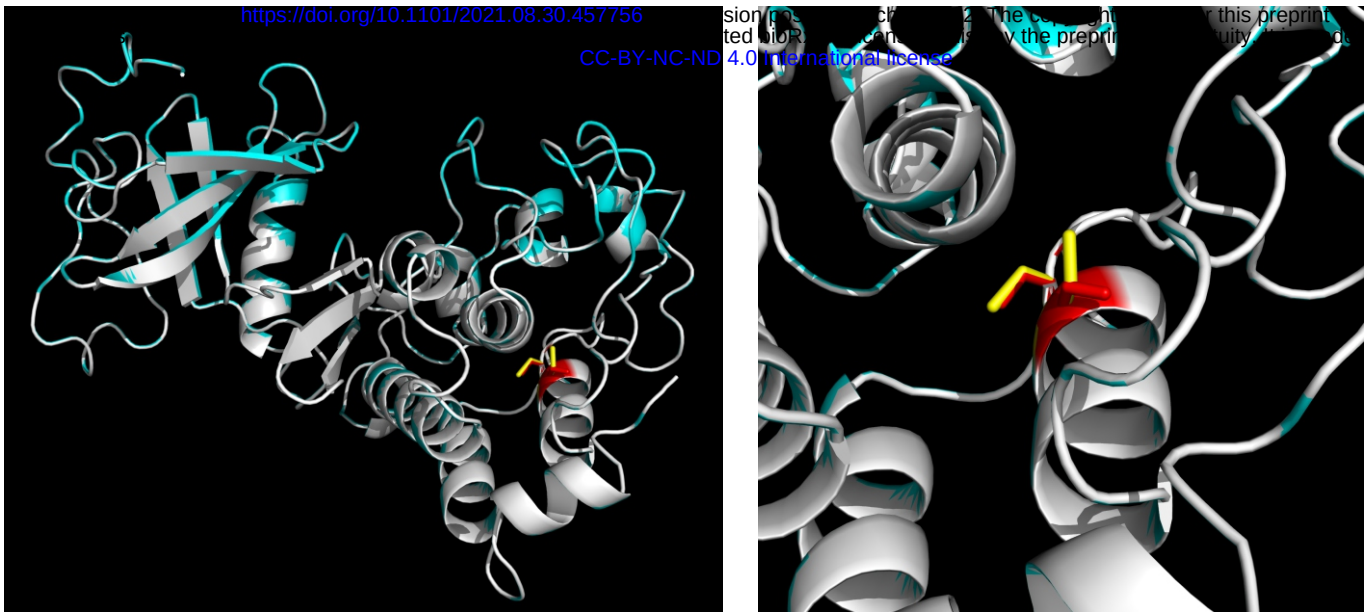

Supplemental figure 4. Mutation of kinase domain S-acylation site cysteines to serine in FLS2 is not predicted to affect kinase domain structure. A. Superimposition of the modelled structures of FLS2 (white) and FLS2 $C^{1132,1135}S$ (blue) kinase domains. **B.** Zoomed in view of Cys1132,1135 in FLS2 (yellow) and substituted serine (red) residues in FLS2 $C^{1132,1135}S$. Only the proton of Ser1132 is predicted to diverge from the FLS2 structure, being rotated by ~110 degrees compared to the original cysteine. This rotation does not affect the position or packing of any other amino acid.